EROs in the EIS fields

I. The AXAF (Chandra) deep field[⋆]

M. Scodeggio[⋆⋆] **and D.R. Silva**

European Southern Observatory, Karl-Schwarzschild-Strasse 2 85748 Garching bei München, Germany
(marcos@ifctr.mi.cnr.it, mscodegg,dsilva@eso.org)

Abstract. The publicly available EIS-DEEP optical-NIR data for the AXAF (Chandra) Deep Field have been used to construct samples of Extremely Red Objects (EROs) using various single-band and multi-band color criteria. In this work we define as EROs objects with colors consistent with passively evolving elliptical galaxies at $z \geq 1$. The EROs surface densities we derive are intermediate between previous published values, emphasizing again the need for larger survey areas to constrain the effects of possible large-scale structure. Although various single-color selected samples can be derived, the EROs sample selected using $R - Ks > 5, I - Ks > 4, J - Ks > 1.8$ jointly is likely to contain the highest fraction of passively evolving luminous field elliptical galaxies at $z \geq 1$, or conversely, the lowest fraction of lower redshift interlopers. The surface density of this multi-band selected EROs sample is consistent with the conclusion that little or no field elliptical volume density evolution has occurred in the redshift range $0 > z > 1.5$. However, extensive spectroscopic followup is necessary to confirm this conclusion.

Key words: galaxies: elliptical and lenticular, cD – galaxies: evolution – galaxies: formation – cosmology: observations

1. Introduction

The formation history of field elliptical galaxies (i.e. elliptical galaxies located outside of massive galaxy clusters) remains very uncertain. Although most stellar population indicators point towards star formation at z > 2, it remains unclear when and how these stars were assembled into their current dynamical structures.

Two formation scenarios with distinct observational predictions continue to be debated. Each one allows for star formation to take place at high redshift, i.e. for the present epoch stellar populations of field ellipticals to be mostly old and metal-rich.

However, the first scenario, based on the *rapid dissipative collapse* model, postulates that the stars were formed and assembled into elliptical galaxies in one rapid collapse event at high (z > 2) redshift (Eggen et al. 1962; Larson 1974; Tinsley & Gunn 1976). In this "top-down" scenario field ellipticals have evolved quiescently since their formation, and therefore the number of massive/luminous field elliptical per co-moving volume should be constant at all redshifts between now and their formation epoch. On the contrary, the opposing *hierarchical merger* scenario assumes that ellipticals were assembled from previously formed sub-units, and that this process has continued until the current epoch (see, e.g. Toomre 1977; White & Rees 1978; Blumenthal et al. 1984). In this "bottom-up" scenario, the number of massive/luminous elliptical field galaxies per co-moving volume increases over time.

These seemingly distinct and easily tested observational predictions have in practice been difficult to resolve at relatively low redshift. Based on the Canada-France Redshift Survey, Lilly et al. (1995) concluded that there has been no significant number evolution for bright, early-type galaxies since z = 1. This result was questioned by Kauffmann et al. (1996), but it has been confirmed by Schade et al. (1999), who took advantage in their study also of the availability of detailed morphological information derived from HST images. Comparing the co-moving number density of field elliptical galaxy at z > 1 to the current epoch number density would be more fruitful because the longer time baseline creates a larger (and therefore easier to detect) number density difference in the hierarchical model. Under the rapid dissipative collapse model, of course, the co-moving number density would remain constant.

The availability of large format near-IR arrays has created the opportunity to search for the luminous field ellipticals at high redshift needed to carry-out this test. These searches are based on a very simple concept: once the 4000 Å break is redshifted beyond the I-band, the observed optical-IR colors of a quiescently evolving elliptical become very red ($R - K > 5; I - K > 4$). In terms of brightness, a typical current epoch field elliptical redshifted to z > 1 will have an observed K of $\approx$ 19–21 (Moustakas et al. 1997). Objects with these extreme properties (faint K-band magnitudes, extremely red optical-NIR colors) are now commonly known as Extremely Red Objects (EROs).

Table 1. Published Deep EROs Survey Results

Reference (1)	Color (2)	Area (3)	$K_{\lim}$ (4)	N(EROs) (5)	N(EROs)/deg^2 (6)
Djorgovski et al. 1995	i–K	3	20	1	1200 ± 1200
Cowie et al. 1996	I–K	26	20	19	2611 ± 600
Moustakas et al. 1997	I–K	2	22	11	$19800^{\mathrm{a}} \pm 6000$
Moustakas et al. 1997	I–K	2	20	3	5400 ± 3100
Barger et al. 1999	I–K	62	20	16	929 ± 230
Cohen et al. 1999	R–K	15	20	19	4560 ± 1050
Thompson et al. 1999	R–K	154	20	289	6750 ± 400
This work	I–K	23	20	20	3130 ± 700
This work	R–K	43	20	22	1842 ± 390
This work	RIJK$^{\mathrm{b}}$	23	20	10	1565 ± 495

Columns: (1) Reference; (2) Color Criteria (R–K > 5 or I–K > 4); (3) Area Surveyed (square arcminutes); (4) K-band EROs Limiting Magnitude; (5) Number of EROs Found; (6) Implied Number of EROs per square degree, with associated Poissonian uncertainty.

[a] Note the different limiting magnitude associated with this EROs density.
[b] This is a multi-color selection criterion, discussed in Sect. 4.

Of course, EROs imaging surveys only measure EROs surface density. Determining the field elliptical galaxies volume density ultimately requires a combination of morphological and spectroscopic information to eliminate Galactic and extragalactic interlopers and to determine the redshifts of high redshift field elliptical galaxy candidates. Although some EROs have been found to have spectral properties consistent with young (3–4 Gyr) elliptical galaxies (e.g., Cowie et al. 1996; Dunlop et al. 1996; Spinrad et al. 1997; Cohen et al. 1999), spectra and/or exact redshifts are available for only a very small fraction (10–15%) of detected EROs. Thus, it is possible that some EROs are in fact dust-enshrouded galaxies at lower redshift (as discussed, e.g., by Graham & Dey 1996; Cimatti et al. 1998) or foreground lower main sequence and brown dwarf stars, although the latter possibility is extremely unlikely given the apparent surface density of such Galactic objects (Moustakas et al. 1997; Cohen et al. 1999). Despite such contamination problems, observed EROs number surface density should be able to place a stringent upper limit on luminous field elliptical galaxy number volume density at $z > 1$.

Unfortunately, published results from such surveys do not present a consistent picture of EROs surface density, let alone inferred volume density. As Table 1 illustrates, measured EROs surface densities vary by factors of 2–6. Clearly, a consensus result has not been reached yet. However, given that most of these surveys cover very small areas, it is not impossible that the observed surface density variations are caused by large-scale structure at high redshift. Additional samples, and preferable over larger areas, are still needed.

In this first in a series of three papers, we present an analysis of the optical-NIR images obtained of the AXAF (Chandra) Deep Field as part of the ESO Imaging Survey (EIS; Rengelink et al. 1999). These data cover an area of approximately 43 square arcmin, comparable in spatial area to the largest EROs surveys already published. The EIS data have been used to construct EROs samples using a variety of magnitude and color crite-

ria. In this paper, we review the EIS dataset (Sect. 2) and then present a number of possible EROs samples using different selection criteria (Sect. 3). The sample most likely to represent field elliptical galaxies at $z > 1$ is then discussed in Sect. 4. Our results are summarized in Sect. 5.

In the next two papers, we will present an analogous analysis of the public EIS-DEEP HDF-S dataset (da Costa et al. 1999) and of a private near-IR dataset obtained as part of two independent EIS Cluster candidate followup surveys. The total area surveyed by this joint study will be ~ 400 square arcmin, i.e. larger than any other published EROs imaging survey at a comparable K-band limiting magnitude.

2. The data

This work is based on the publicly available data obtained as part of the ESO Imaging Survey (EIS) on the so-called AXAF (Chandra) Deep Field, at $\alpha = 03^h 32^m 30^s$ and $\delta = -27°48'30''$. Deep multi-band optical and infrared observations in this field were obtained in the period August-November 1998, using the ESO 3.5m New Technology Telescope (see Rengelink et al. 1999 for details). Optical observations in the $UBVRI$ bands were carried out with the SUSI2 camera (D'Odorico et al. 1998), equipped with two $4k \times 2k$ EEV CCDs, covering a field of view of 5.46×5.46 arcmin with a pixel scale of 0.16 arcsec/pixel (after 2×2 binning). Infrared observations in the J and Ks bands were carried out using the SOFI infrared camera and spectrograph (Moorwood et al. 1998), equipped with a Rockwell $1k \times 1k$ detector, covering a field of view of 4.9×4.9 arcmin with a pixel scale of 0.29 arcsec/pixel.

The infrared observations cover 4 SOFI fields, for a total area of approximately 83 square arcmin. Optical observations at the moment cover only the two northern SOFI fields, for a total area of approximately 56 square arcmin, except in the I band, where only a smaller 30 square arcmin area has been covered. Total exposure times are 5500 seconds for the V- and R-band

exposures, 12600 seconds for the I-band exposure, and 10800 seconds for the J- and Ks-band exposures. Details about the data reduction procedures are given by Rengelink et al. (1999), and da Costa et al. (1999), and only a brief summary is presented here. Single dithered optical exposures were coadded using the drizzle procedure (Fruchter & Hook 1998) implemented within the EIS pipeline. Infrared jittered images were combined using the *jitter* program within the Eclipse data-reduction package (Devillard 1998). The final single-band coadded images were astrometrically calibrated using the USNO-A V1.0 catalog as a reference. The photometric calibration was based on observations of Landolt (1992) standard stars for the optical data, and of HST standards from the list of Persson et al. (1998) for the infrared data. Zero-point uncertainties are of ±0.03 mag in V-band, ±0.04 mag in R-band, and of ±0.05 mag in I-, J-, and Ks-band.

A multi-color object catalog was created based on the method of the chi-squared image, described by Szalay et al. (1999). All single-band coadded images were convolved with a Gaussian kernel to devise a set of images with homogeneous PSFs (i.e. equivalent to the single-band image with worse seeing, the I-band image), normalized by their respective *rms* noise values, and then quadratically combined to obtained a chi-squared image. Object detection on that image was carried out using the SExtractor software (Bertin & Arnouts 1996). Magnitude measurements based on the detection parameters derived from the chi-squared image were performed on the Gaussian convolved single-band coadded images.[1] Magnitudes were then measured within a 4 arcsec diameter aperture. From a comparison with deep number counts in the literature, it is estimated that the 90% completeness limit of the multicolor catalog in the different bands is approximately $V = 26.2$, $R = 26.0$, $I = 25.6$, $J = 23.6$, $Ks = 21.6$ (see da Costa et al. 1999, and Rengelink et al. 1999). Star/galaxy separation was based on the SExtractor stellarity index, considering as galaxies object with index ≤ 0.85, when measured in the Ks-band images. It is important to remark that this classification criterion is reliable only for galaxies at least 1–1.5 mag brighter than the detection limit. Stellar contamination is however expected to be very limited at this galactic latitude ($b \simeq -55$), and our selection of very red objects is expected to reduce it even further (see for example da Costa et al. 1999).

In this work, we restrict ourselves to the area covered by both the optical and infrared observations, and further limit our analysis to the area where the sensitivity of the single-band coadded images is most uniform, rejecting those parts of the surveyed area where the sensitivity is below 75% of the peak in any of the single-band coadded images. In this way, the area we consider covered by the $RJKs$ observations is ~ 43 square arcmin, while that covered by the $RIJKs$ observations is $\sim$

---

[1] Our final catalog differs somewhat, especially at the faintest magnitude, from the AXAF Deep Field catalogs released by the EIS Team in December 1998 on their Web site. When constructing the December 1998 catalogs, the coadded single-band images were not convolved by a Gaussian before the chi-square image was constructed and object magnitudes were measured on the non-convolved single-band images.

23.5 square arcmin. Within these areas we derive an object catalog by selecting all objects measured above the 2σ limit in the Ks-band, which in practice limited us to objects brighter than $Ks = 21.0$. At that Ks limiting magnitude, the equivalent limiting magnitudes in our other bands were $J = 22.8$, $I = 25.0$, and $R = 26.0$ with magnitude uncertainties of approximately 0.1 mag in R, and 0.15 mag in I, J, and Ks.

3. Single-color selected EROs samples

As our main objective is to study the evolution of the volume density of $z > 1$ field elliptical galaxies, we define EROs to be color-selected objects that are redder than a z $\simeq 1$ passively evolving elliptical galaxy. While this definition has been already used by other authors (e.g., Barger et al. 1999, Cohen et al. 1999), it is not unanimously adopted in the literature, as other studies have defined EROs to be objects that are redder than a passively evolving elliptical galaxy at any redshift (e.g., Andreani et al. 1999, Thompson et al. 1999). Since most previously published studies have relied on a single color criterion to select EROs, we decided to select from our dataset a number of different single color samples, based on the criteria $R - K \geq 5.0$, $I - K \geq 4.0$, or $J - K \geq 1.8$. We make no use of the available V-band data since it is too shallow for our requirements (the color criterion would be $V - K \geq 7.0$, which would require completeness down to $V = 28$). These criteria were designed to include in the samples all the elliptical galaxies at $z \geq 1$ that would have properties comparable to those of their present-day counterparts, taking into account the passive evolution of their stellar population (assumed to have formed at $z > 2$). At the same time, these choices allow comparisons with previously published EROs surveys to be readily carried out, although the effective redshift cutoff for passively evolving early-type galaxies might be slightly different for the different colors, as the color-color tracks plotted in Fig. 1 show. The effect however is very small, and does not significantly affect the analysis carried out in this paper.

Obviously a single color measurement is not enough to define, even approximately, a galaxy's spectral energy distribution (SED). Therefore every EROs sample that is defined on the basis of a single-color criterion is likely to contain both $z \geq 1$ early-type galaxies and a mixture of other objects, including dusty star-forming galaxies, and low-mass stars. Moreover, as illustrated in Fig. 1, samples constructed from such single color criteria will not only include early-type galaxies, but may also contain even normal early-type spiral galaxies at $z \sim 1.6 - 1.8$. The largest contamination is expected to be present in the $J - K \geq 1.8$ sample, given the relatively small range of $J - K$ color observed among galaxies of all morphological types. As discussed above, only after obtaining spectroscopic and morphological information it will be possible to produce a sample of bona fide high redshift field elliptical galaxies.

Using the multi-band observations in the AXAF (Chandra) Deep Field described in the previous section, we cover a large enough area to derive a reliable estimate of the EROs surface
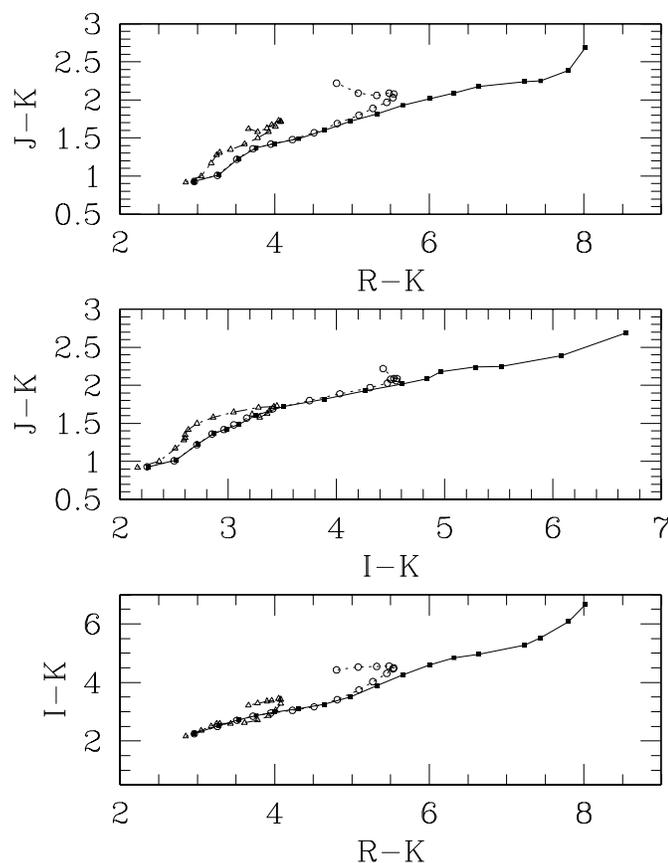
Table 2. EROs samples selected using different color criteria

Ks^{lim}	N($< Ks^{lim}$)	N($J - Ks > 1.8$)	N($R - Ks > 5.0$)	N($R - Ks > 6.0$)
		$RJKs$ area (43 square arcmin)		
19.0	185	30	4	1
19.5	270	57	16	2
20.0	362	87	22	4
20.5	488	122	36	8
21.0	692	190	54	17
Ks^{lim}	N($< Ks^{lim}$)	N($I - Ks > 4.0$)	N($I - Ks > 5.0$)	N($R - Ks > 5.0$)
		$RIJKs$ area (23.5 square arcmin)		
19.0	99	5	0	3
19.5	149	14	0	9
20.0	200	20	2	11
20.5	280	33	8	21
21.0	397	56	11	30

Fig. 1. Color–color tracks for galaxies with different star formation histories. The observed colors as a function of galaxy redshift, in the interval $0 < z < 2$, are plotted for an elliptical galaxy (solid line, filled squares), an early-type spiral (dotted line, open circles), and a late-type spiral (dashed line, open triangles). The dots identify redshift intervals $\Delta z = 0.1$, starting from the bottom-left in each panel. The colors are computed using population synthesis models from Bruzual & Charlot (1993), assuming an H$_0$=75 km s^{-1}Mpc^{-1}, $\Omega_0 = 0.3$ cosmological model, Salpeter IMF, and solar metallicity for all galaxies.

density to different limiting magnitudes, and we can also compare the results obtained adopting different selection criteria. Table 2 presents an overview of the different samples we have extracted from the available data using single-color criteria.

The properties of the total sample of Ks-selected objects agree quite well with those of previously published samples. Over the magnitude interval $19.5 \leq Ks \leq 21.0$ the logarithmic slope of the objects number counts is approximately 0.27, comparable to those derived by Moustakas et al. (1997), by Djorgovski et al. (1995), and by Gardner, Cowie & Wainscoat (1993). The surface density of objects brighter than $Ks = 20.0$ is approximately 8.5 arcmin^{-2}, intermediate between those derived by Moustakas et al. (1997) and by Cowie et al. (1996), and that reported by Djorgovski et al. (1995). We note that the most discrepant densities with respect to the one measured here, those reported by Moustakas et al. (1997) and by Djorgovski et al. (1995), were obtained from observation covering an area less than one twentieth of that used in this work.

The exact nature of EROs is still very uncertain because they are only detected at relatively faint infrared magnitudes, and are therefore extremely faint at optical wavelengths because of their red colors (see, for example, Fig. 9 in Cowie et al. 1996). We find that all three EROs selection criteria adopted here produce samples that are significantly underpopulated of bright objects, with respect to the total sample of Ks-selected objects. The logarithmic slope of the number counts of $J - Ks > 1.8$, $I - Ks > 4.0$, and $R - Ks > 5.0$ objects are 0.34, 0.39, and 0.36 respectively, over the $19.5 \leq Ks \leq 21.0$ magnitude interval. There are no EROs in our samples brighter than $Ks = 18$. This fact, coupled with the observation that the average color of the galaxy population shows a definite blueing trend at these faint magnitudes (resulting from a stronger star formation activity in $z \sim 1$ galaxies when compared to local ones), and that redshift surveys limited to $K = 18$ do not include any $z > 1$ objects (Songaila et al. 1994; Cohen et al. 1999), can be considered as strong circumstantial evidence in favor of EROs being, for the most part, quiescent high redshift objects.

Table 3. Comparison between single- and multi-color EROs selection criteria

Ks_{lim}	$RIJKs$ area (23.5 square arcmin)			
	N($J - Ks > 1.8$)	N($I - Ks > 4.0$)	N($R - Ks > 5.0$)	N(E,$z > 1$)
19.0	15	5	3	3
19.5	25	14	9	8
20.0	39	20	11	10
20.5	64	33	21	17
21.0	100	56	30	23

The infrared criterion $J - Ks > 1.8$ appears to be the least restrictive of the criteria used to define EROs, producing a sample of 87 (190) objects brighter than Ks of 20.0 (21.0) over the 43 square arcmin covered by the $RJKs$ observations. The corresponding surface brightness is 2.0 (4.5) objects per square arcmin. On the contrary, the $R - Ks > 5.0$ criterion appears to be the most restrictive one, producing a sample of 22 (54) objects brighter than Ks of 20.0 (21.0) over the same area, that correspond to a surface density of 0.5 (1.2) objects per square arcmin. The $I - Ks > 4.0$ criterion produces a sample size intermediate between the previous two sample sizes. This sample is composed of 20 (56) objects brighter than Ks of 20.0 (21.0) over the 23.5 square arcmin covered by the $RIJKs$ observations. The corresponding surface density is 0.8 (2.4) objects per square arcmin. The more extreme $R - Ks > 6.0$ and $I - Ks > 5.0$ selection criteria produce samples of 4 (17) and 2 (11) objects brighter than Ks of 20.0 (21.0), corresponding to surface densities of approximately 0.1 (0.45) objects per square arcmin.

It is clear from the comparison with previously published EROs surveys that the measurement of their average surface density is still affected by large uncertainties, most likely due to the combined effect of the large-scale clustering and small survey areas (see Table 1). The surface density of $R - Ks > 5.0$ objects brighter than $Ks = 20.0$ that we have derived is smaller by a factor of 2.5 than that reported by Cohen et al. (1999), measured over an area approximately one third as large as the one we use in this work. At the same time we find a surface density of $I - Ks > 4.0$ objects brighter than $Ks = 20.0$ more than three times higher than that measured by Barger et al. (1999) over an area approximately three times as large as the one we use. Assuming Poisson statistics are the only source of uncertainty in the measurements, these differences are both significant at approximately the 3σ level (99.36% and 99.75% significance level, respectively). We remark that both those studies are based on samples limited to a K-band magnitude of 20.0, and therefore the corresponding densities of EROs could be affected by subtle "edge of the catalog" effects. A good agreement is found instead with the density of $I - Ks > 4.0$ objects measured by Cowie et al. (1996) over an area of similar extent to the one we use here.

Taken all together these results indicate that it might be premature to derive any conclusion on the density evolution and on the formation epoch of elliptical galaxies from the currently available EROs surveys. For example, based on their $I - K$

selected sample, Barger et al. (1999) concluded that volume density of high-z field ellipticals could be no more than 50% of the current epoch volume density. But as Table 1 illustrates, using similar selection criteria, we derive an EROs surface density three times larger than the Barger et al. result. Simply scaling by the implied Barger et al. surface-to-volume density ratio, our analogous upper limit on high-z field ellipticals is larger than the current epoch value. Only measuring the true redshift distribution of both samples will resolve this contradiction.

4. A multi-color selected EROs sample

In the previous section, we discussed EROs samples constructed using a single-color criterion. Such single-color samples will obviously contain interlopers to a greater or lesser degree for one simple reason: one color is not enough to uniquely determine the complete SED of any given object. This simple fact has driven modern photometric redshift surveys to increasing numbers of filters to more accurately constrain the measured SED (e.g., Koo 1985). In a similar vein, we can use the three colors available to us ($R - K$, $I - K$, and $J - K$) to construct an EROs sample which should have a higher yield of actual high-redshift elliptical galaxies. We are applying a very straightforward principle here: high-redshift (z > 1) passively evolving luminous ellipticals will tend to satisfy all three criteria simultaneously while most sample interlopers (e.g., dusty starburst galaxies, M-type dwarf stars) will not. Therefore, our $RIJK$ sample will better constrain the high-redshift elliptical galaxy volume density upper limit, although it might still contain a number of early-type spiral galaxies with redshift $z \sim 1.6$–1.8, as discussed in the previous section.

Table 3 presents the results of the application of the multi-color criteria to the object catalog from the area covered by the $RIJKs$ observations, and compares it with the results of the application of the single-color criteria. We identify a sample of 10 (23) objects brighter than $Ks = 20.0$ (21.0) that satisfy all three color criteria, over an area of 23.5 square arcmin. This corresponds to a surface density of 0.4 (1.0) objects per square arcmin. This density, although significantly smaller than the $I - Ks > 4$ sample, is still approximately 1.6 times higher than that reported by Barger et al. (1999). Using the Barger et al. surface-to-volume density ratio again, we could conclude that our $RIJK$ selected sample implies a high-redshift volume density comparable to the current volume density, i.e. that significant number evolution has not occurred since z $\sim$ 1.5.
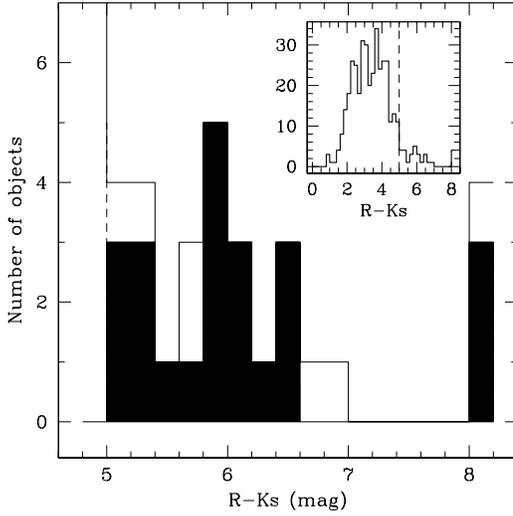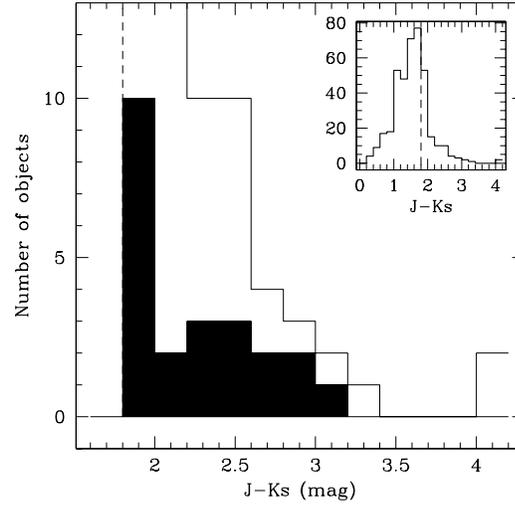
Fig. 2. The $R - Ks$ color distribution for $Ks \leq 21, R - Ks > 5$ objects in the area covered by the $RIJK$ data (open histogram) compared to the color distribution of the objects selected using the more restrictive $RIJK$ criteria (shaded histogram). The latter objects are the most likely candidates for $z > 1$ passively evolving elliptical galaxies. The inset shows the color distribution for the entire $Ks \leq 21.0$ sample in the same area. The vertical dashed line indicates the $R - Ks > 5.0$ single-band EROs selection criterion. For all histograms, the bin size is 0.2 mag. Objects in the reddest bin represent non-detections in the R-band, and are given an arbitrary very red color purely for display purposes.
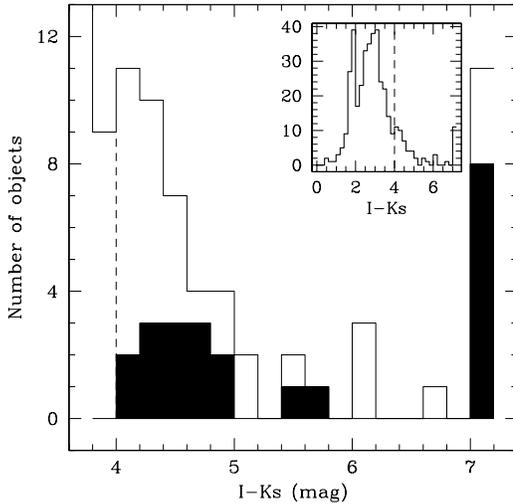
Fig. 3. The $I - Ks$ color distribution for $Ks \leq 21, I - Ks > 4$ objects in the area covered by the $RIJK$ data (open histogram) compared to the color distribution of the objects selected using the more restrictive $RIJK$ criteria (shaded histogram). The latter objects are the most likely candidates for $z > 1$ passively evolving elliptical galaxies. The notation is the same as in the previous figure. The inset shows the color distribution for the entire $Ks \leq 21.0$ sample in the same area. The vertical dashed line indicates the $I - Ks > 4.0$ selection criterion. Objects in the reddest bin represent non-detections in the I-band.

We can also use our multi-band selected sample to quantify the likely contamination fraction in the single-band selected

Fig. 4. The $J - Ks$ color distribution for $Ks \leq 21, J - Ks > 1.8$ objects in the area covered by the $RIJK$ data (open histogram) compared to the color distribution of the objects selected using the more restrictive $RIJK$ criteria (shaded histogram). The latter objects are the most likely candidates for $z > 1$ passively evolving elliptical galaxies. The notation is the same as in the previous figure. The inset shows the color distribution for the entire $Ks \leq 21.0$ sample in the same area. The vertical dashed line indicates the $J - Ks > 1.8$ selection criterion. Objects in the reddest bin represent non-detections in the J-band.

samples discussed in the last section. Consider Table 3 and Figs. 2– 4. Recall that all four bands are only available for the $\sim$ 23.5 square arcmin area. To a limiting magnitude of $Ks = 21.0$, the 23 very likely $z > 1$ passively evolving elliptical galaxies are extracted from samples of 30 $R - Ks \geq 5.0$ objects (77% efficiency); 56 $I - Ks \geq 4.0$ objects (41% efficiency) and 100 $J - Ks \geq 1.8$ objects (23% efficiency). The level of contamination is therefore very low in the $R - Ks \geq 5.0$ sample (around 20%), and increases dramatically when we move to colors based on filters with a smaller wavelength difference between them, reaching approximately 75% level for the $J - Ks > 1.8$ sample.

Can we conclude that $R - Ks > 5.0$ is the best criterion to search for high-redshift ellipticals when no other information is available? This question will be addressed further in Papers 2 and 3, as we study other EROs samples and do a more extensive color plane analysis of possible contaminating populations using spectral synthesis models.

We close by remarking that there is no evidence for high-redshift clusters in the 23.5 square arcmin area covered by our $RIJK$ selected sample. However, there appears to be one high-redshift cluster candidate in the total RJK area. This topic is discussed more extensively in Scodeggio et al. (2000, in preparation).

5. Summary

We have used the publicly available EIS-DEEP optical-NIR data for the AXAF (Chandra) Deep Field to construct samples of Extremely Red Objects (EROs) using various color criteria

consistent with passively evolving elliptical galaxies at $z > 1$. Our conclusions can be summarized as follows:

1. The surface density of EROs is still far from being reliably determined, and there are significant differences in different surveys. The EROs surface densities derived here lie between the values derived for other studies. A larger, and preferably non-contiguous, area should be used to better constrain EROs surface density.

2. Just one color measurement is not enough to select accurately likely $z > 1$ elliptical galaxies. However, if obtaining more than one color is impossible or undesirable for some reason, our results suggest that $R - K$ is the most efficient color to use. We will study this issue further in our next paper.

3. We have used multi-band EROs selection criterion to construct a sample of likely $z > 1$ passively evolving elliptical galaxies. Our derived surface density is consistent with little or no volume density of such objects since $z \sim 1.5$. This result is tenuous, as well as being based on very simple arguments, and requires spectroscopic followup to confirm the nature of the multi-band selected EROs population.

References

Andreani P., Cimatti A., Röttgering H., Tilanus R., 1999, astro-ph/9903121

Barger A.J., Cowie L.L., Trentham N., et al., 1999, AJ 117, 102

Bertin E., Arnouts S., 1996, A&AS 117, 393

Blumenthal G.R., Faber S.M., Primack J.R., Rees M.J., 1984, Nat 311, 517

Bruzual A.G., Charlot S., 1993, ApJ 405, 538

Cimatti A., Andreani P., Röttgering H., Tilanus R., 1998, Nat 392, 895

Cohen J.G., Blanford R., Hogg D.W., Pahre M.A., Shopbell P.L., 1999, ApJ 512, 30

Cowie L.L., Songaila A., Hu E.M., Cohen J.G., 1996, AJ 112, 839

da Costa L., Nonino M., Rengelink R., et al., 1999, A&A, in press (astro-ph/9812105)

Devillard N., 1998, Eclipse Data Analysis Software Package (ESO: Garching)

Djorgovski G.S., Soifer B.T., Pahre M.A., et al., 1995, ApJ 438, L13

D'Odorico S., Beletic J.W., Amico P., Hook I., Marconi G., Pedichini F., 1998, Proc. SPIE 3355, 507

Dunlop J., Peacock J., Spinrad H., et al., 1996, Nat 381, 581

Eggen O.J., Lynden-Bell D., Sandage A., 1962, ApJ 136, 748

Fruchter A.S., Hook R.N., 1998 (astro-ph/9808087)

Gardner J.P., Cowie L.L., Wainscoat R.J., 1993, ApJ 415, L9

Graham J.R., Dey A., 1996, ApJ 471, 720

Kauffmann G., Charlot S., White S.D.M., 1996, MNRAS 283, L117

Koo D., 1985, AJ 90, 418

Landolt A.U., 1992, AJ 104, 340

Larson R.B., 1974, MNRAS 166, 585

Lilly S.J., Tresse L., Hammer F., Crampton D., LeFevre O., 1995, ApJ 455, 108

Moorwood A., Cuby J.G., Lidman C., 1998, The ESO Messenger 91, 9

Moustakas L.A., Davis M., Graham J.R., et al., 1997, ApJ 475, 445

Persson S.E., Murphy D.C., Krzeminski W., Roth M., Rieke M.J., 1998, AJ 116, 2475

Rengelink R., Nonino M., da Costa L., et al., 1999, A&A, in press (astro-ph/9812190)

Schade D., Lilly S.J., Crampton D., et al., 1999, ApJ 525, 31

Songila A., Cowie L.L., Hu E.M., Gardner J.P., 1994, ApJS 94, 461

Spinrad H., Dey A., Stern D., et al., 1997, ApJ 484, 581

Szalay A.S., Connoly A.J., Szokoly G.P., 1999, AJ 117, 68

Thompson D., Beckwith S.V.W., Fockenbrock R., et al., 1999, ApJ 523, 100

Tinsley B.M., Gunn J.E., 1976, ApJ 203, 52

Toomre A., 1977, in: Tinsley B.M., Larson R.B. (eds.), The Evolution of Galaxies and Stellar Populations. New Haven: Yale Univ. Obs., p. 401

White S.D.M., Rees M.J., 1978, MNRAS 183, 341